RSC Advances

PAPER

View Article Online
View Journal | View Issue

Cite this: *RSC Adv.*, 2017, **7**, 52151

Electrochemical properties of lithium–titanium oxide, modified with Ag–Cu particles, as a negative electrode for lithium-ion batteries

Michal Krajewski,[a] Bartosz Hamankiewicz,[*ab] Monika Michalska,[c] Mariusz Andrzejczuk,[d] Ludwika Lipinska[c] and Andrzej Czerwinski[*ae]

Received 25th September 2017
Accepted 5th November 2017

DOI: 10.1039/c7ra10608d

rsc.li/rsc-advances

Composites of $Li_4Ti_5O_{12}$ with Ag–Cu particles were successfully synthesized by solid-state reaction followed by thermal decomposition of the metal substrates. The presence of metallic particles was confirmed by X-ray diffraction, scanning transmission electron microscopy and X-ray photoelectron spectroscopy. Galvanostatic charge–discharge tests showed improved specific capacity and capacity retention of $Li_4Ti_5O_{12}$/Ag–Cu composites at a 10C current rate, while cyclic voltammetry and electrochemical impedance spectroscopy revealed changes in Li^+ ion chemical diffusion coefficient values and charge-transfer resistance with increasing amount of Ag–Cu in prepared powders. The synthesis and structural, morphological and electrochemical evaluation of $Li_4Ti_5O_{12}$/Ag–Cu powders, carried out in this work, were also presented here for the first time.

1. Introduction

One of the candidates to replace graphite as an anode material in lithium-ion batteries is lithium–titanium oxide ($Li_4Ti_5O_{12}$, LTO) of spinel structure. It shows excellent cyclability due to negligible volume change during intercalation/deintercalation reactions (so called "zero-strain" electrode material).[1,2] A high operating potential of 1.55 V *vs.* Li^+/Li^0 is responsible for LTO's enhanced safety, due to hindering the formation of a Solid Electrolyte Interface (SEI) layer on the electrode's surface, although some research groups reported SEI creation as a result of spontaneous reactions with the electrolyte or migration of SEI components formed on counter electrodes.[3,4] $Li_4Ti_5O_{12}$ has an acceptable specific capacity of 175 mAh g^{-1} when charged/discharged in the potential range of 1.00–3.00 V (*vs.* Li^+/Li^0) when the following reaction occurs:

$$Li_4Ti_5O_{12} + 3Li^+ + 3e^- \leftrightarrow Li_7Ti_5O_{12}, \quad (1)$$

and 293 mAh g^{-1} while expanding the potential window to 0.01–3.00 V (*vs.* Li^+/Li^0). Increased capacity of lithium–titanium oxide when cycled to 0.01 V is related to full reduction of titanium ions from +4 to +3 oxidation state which involves additional two Li^+ ions:[5]

$$Li_7Ti_5O_{12} + 2Li^+ + 2e^- \leftrightarrow Li_9Ti_5O_{12}. \quad (2)$$

All mentioned properties make LTO a good material for next generations of Li-ion batteries. However, due to low electric conductivity of $Li_4Ti_5O_{12}$, its widespread application is still limited.[6–8]

Many approaches were suggested to improve the electrochemical performance of electrode materials for lithium-ion batteries which included, among others, carbon coating,[9] ion doping,[10] surface modifying[11,12] or even electrode design.[13] In $Li_4Ti_5O_{12}$ case, to enhance its electrochemical properties, many research groups tried various synthetic routes (such as solid-state,[14–18] sol–gel,[19–23] hydrothermal,[24–28] combustion,[29–31] microwave,[32–34] spray pyrolysis,[35,36] or atomic layer deposition[37]), cation (Mg^{2+},[38,39] Ni^{2+},[40] Al^{3+},[41–43] Cr^{3+},[44,45] Zr^{4+},[46–48] V^{5+},[49,50] Nb^{5+},[51] Ta^{5+},[52]) and anion (Br^-,[53,54] F^-,[41,55,56]) doping or surface modification with conductive materials (carbon coat,[57–61] graphene/graphene oxide,[62–65] carbon nanotubes,[66–68] Ag,[69–79] Cu,[80–84] Au,[85] TiN[86–88]).

In our previous studies, we synthesized and fully characterized $Li_4Ti_5O_{12}$ modified with silver nanoparticles.[78,79] The deposition of Ag nanoparticles highly enhanced electrochemical properties of lithium–titanium oxide, such as cyclability, high-rate performance and intercalation/deintercalation reaction kinetics. Due to the fact, that silver is considered as an "expensive" metal, in this work we focused on reducing the amount of Ag by incorporating a metal from the same periodic table's group into LTO powders, which is less costly and highly

[a]Faculty of Chemistry, University of Warsaw, Pasteura 1, 02-093 Warsaw, Poland. E-mail: aczerw@chem.uw.edu.pl; bhamankiewicz@chem.uw.edu.pl
[b]Biological and Chemical Research Centre, University of Warsaw, Zwirki i Wigury 101, 02-089 Warsaw, Poland
[c]Institute of Electronic Materials Technology, Wolczynska 133, 01-919 Warsaw, Poland
[d]Faculty of Materials Science Engineering, Warsaw University of Technology, Woloska 141, 02-507 Warsaw, Poland
[e]Industrial Chemistry Research Institute, Rydygiera 8, 01-793 Warsaw, Poland

conductive, obtaining and fully characterizing a cheaper, silver–copper composite of $Li_4Ti_5O_{12}$ with enhanced electrochemical properties in lithium-ion batteries.

2. Experimental

2.1 Synthesis of pristine $Li_4Ti_5O_{12}$

The one-step solid-state synthesis was used to obtain single-phase lithium–titanium oxide powder of spinel structure. The synthesis was carried out under high-energy ball-milling (HEBM) process, using ethanol as a medium and zirconia balls, in a Planetary Mono Mill PULVERISETTE 6 (Fritsch, Germany). The starting reagents used were titanium dioxide (TiO_2, 99%, Sigma-Aldrich) mixed with lithium carbonate (Li_2CO_3, synthesized in-house, at the Institute of Electronic Materials Technology) at the Ti : Li molar ratio of 5 : 4. The high-energy ball-milling process was carried out at a constant speed of 200 rpm and processing time of 12 h, respectively. Following the ball-milling process, the remaining alcohol medium was evaporated and the obtained powder was subsequently dried at 150 °C for a few hours in air atmosphere. Finally, the powder was ground in an agate mortar and heat-treated in air: a two-stage thermal treatment, consisting of 6 h annealing at 500 °C followed by 20 h annealing at 800 °C, was employed.[18]

2.2 Synthesis of $Li_4Ti_5O_{12}$/Ag–Cu composites

To synthesize the $Li_4Ti_5O_{12}$/Ag–Cu composites, $AgNO_3$ (Avantor Performance Materials Poland S.A.) and $Cu(NO_3)_2 \cdot 3H_2O$ (Chempur) were firstly dissolved in an ethanol solution, separately. The nitrate–ethanol solutions of Ag and Cu were mixed together. Then, the prepared nanocrystalline $Li_4Ti_5O_{12}$ powder was added to the silver–copper nitrate solution to obtain a suspension. In subsequent processes the weight ratio of Ag : Cu (equal volume) and LTO was 0.005 : 0.005, 0.01 : 0.01, 0.015 : 0.015, 0.02 : 0.02 and 0.025 : 0.025, respectively. The mixture was magnetically stirred for a few hours to obtain a homogenously dispersed suspension and then was dried in air for a few hours at 150 °C. At the last step, the composites were ground in an agate mortar to obtain a fine powder.[78,79]

2.3 XRD, SEM, STEM, XPS

Phase identification of the prepared samples was carried out by X-ray diffraction (XRD) using an X-ray Powder Diffractometer Siemens D-500. X-ray profiles were measured between 10 and 60° (2θ angle) with a Cu Kα radiation source ($\lambda = 1.542$ Å).

Scanning electron microscopy (SEM) was used to study the microstructure of the surface modified LTO powders. Samples were prepared by dispersing a small portion of dry powders on a conductive carbon tape and were investigated on Hitachi S5500 (Hitachi High Technologies Corporation, Japan) scanning electron microscope using backscattered electron (BSE) detector. Scanning transmission electron microscope Hitachi-HD2700 (STEM), operated at 200 kV and equipped with energy dispersive X-ray spectrometer (EDS) was used for more detailed microstructural analysis. Bright Field STEM and High Angle Annular Dark Field STEM modes were used for imaging.

X-ray photoelectron spectroscopy (XPS) experiments have been performed using Kratos Axis Supra instrument with Al Kα monochromatic beam (1486.7 eV) as an X-ray source. The X-ray takeoff angle was set to standard 45°. Pass energy was set to 160 eV and 20 eV for low and high resolution spectra acquisition respectively, providing an energy resolution of ~7.5 and ~0.8 eV respectively. Data treatment was performed within the ESCA software. Curve fitting was achieved by using standard Shirley background subtraction and Gaussian/Lorentzian peak shapes. All spectra were calibrated by using C 1s adventitious carbon as a reference binding energy (284.8 eV).

2.4 Electrochemical measurements

For electrochemical measurements, the electrodes were made of $Li_4Ti_5O_{12}$/Ag–Cu composite ground with Vulcan XC72R (Cabot) carbon in an agate mortar for 20 min. The obtained powder was added to 5% solution of polyvinylidene fluoride (Alfa Aesar) in *N*-methyl pyrrolidinone (Sigma-Aldrich) and the mixture was homogeneously stirred for 4 h. Such prepared slurry was uniformly coated onto copper foil using Elcometer® 3545 and dried in 55 °C for 1 h in air and 120 °C overnight in vacuum. Round electrodes were then cut from the foil and pressed in hydraulic press under 200 bar pressure for 1 min followed by vacuum drying at 120 °C for 16 h. The electrode composition was 8 : 1 : 1 wt ratio of $Li_4Ti_5O_{12}$/Ag–Cu : PVdF : carbon. The cells were assembled in an argon-filled glove-box (MBraun Unilab MB-20-G).

The electrochemical tests were carried out in three-electrode Swagelok®-type cells with $Li_4Ti_5O_{12}$/Ag–Cu working electrode, lithium metal foil (Sigma-Aldrich) as a reference and a counter electrodes, a porous polymer separator (Celgard® 2400) and liquid electrolyte mixture containing 1 M $LiPF_6$ in ethylene and dimethyl carbonate (1 : 1 wt/wt) solvents (BASF). The chronopotentiometry (CP) experiments were performed using

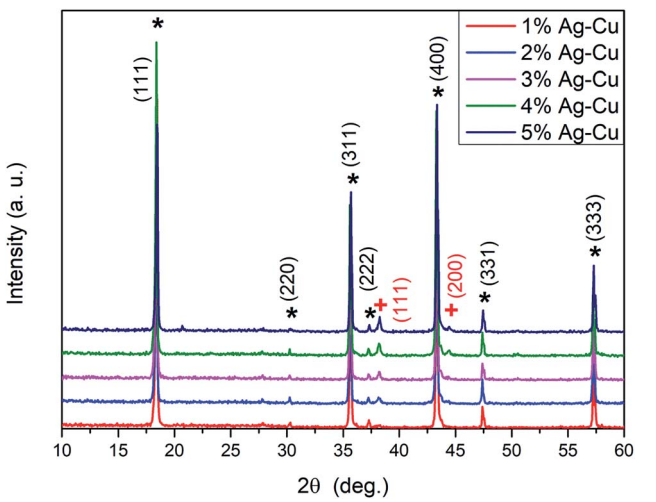

Fig. 1 XRD patterns of $Li_4Ti_5O_{12}$/Ag–Cu composites (* – $Li_4Ti_5O_{12}$, + – Ag).

Table 1 Crystallite sizes and lattice parameters for $Li_4Ti_5O_{12}$/Ag–Cu composites obtained from XRD measurements

Ag–Cu content [%]	Average crystallite sizes [nm] (±5 nm)	Lattice parameter [Å] (±0.001 Å)
1	81	8.358
2	90	8.359
3	85	8.357
4	81	8.357
5	64	8.354

a multichannel battery tester Sollich ATLAS 1361. All examined cells were preliminarily discharged at current rate of 0.1C (C corresponds to current density of 175 mA g^{-1}). Then, the cyclability and high-rate tests were performed. For cyclability tests, the cells were charged/discharged at constant current rate of 1C for 50 consequent cycles. For high-rate tests, the cells were charged at constant current rate of 1C and were discharged at current rates of 1, 2, 5 and 10C for 5 cycles each. All the cells were cycled in 1.00–3.00 V potential range (*vs.* Li^+/Li^0). After high-rate tests, the cells were examined by cyclic voltammetry (CV) and electrochemical impedance spectroscopy (EIS) using CHI760d electrochemical workstation. The CV measurements were performed in the potential range of 1.00–2.20 V (*vs.* Li^+/Li^0) at scan rates of 0.1, 0.2, 0.5, 1.0 and 2.0 mV s^{-1}. The EIS experiments were performed at the potential of 1.00 V (after one hour of cell conditioning) with the amplitude of 10 mV in 10^{-2}–10^5 Hz frequency range. The EIS spectra were analyzed using ZView2 software. For the lithium ion diffusion coefficient calculations, for both CV and EIS tests, the geometric surface area of the electrodes was used.

3. Results and discussion

3.1 XRD, SEM, STEM, XPS

Fig. 1 depicts the XRD patterns of the Ag–Cu modified $Li_4Ti_5O_{12}$ powders. All the peaks from each sample associated with lithium–titanium oxide are in good agreement with the spinel phase $Li_4Ti_5O_{12}$ pattern (ICDD-49-0207) confirming, that modifying the surface using Ag–Cu nanoparticles of pristine $Li_4Ti_5O_{12}$ does not lead to any phase segregation. As presented in Fig. 1 all seven characteristic XRD peaks observed for $Li_4Ti_5O_{12}$/Ag–Cu powders at the 2θ angles of: 18.35, 30.21, 35.60, 27.24, 43.28, 47.39 and 57.27° correspond to the (111), (220), (311), (222), (400), (331) and (333) crystal planes of the cubic structure of lithium–titanium oxide (ICDD-49-0207),

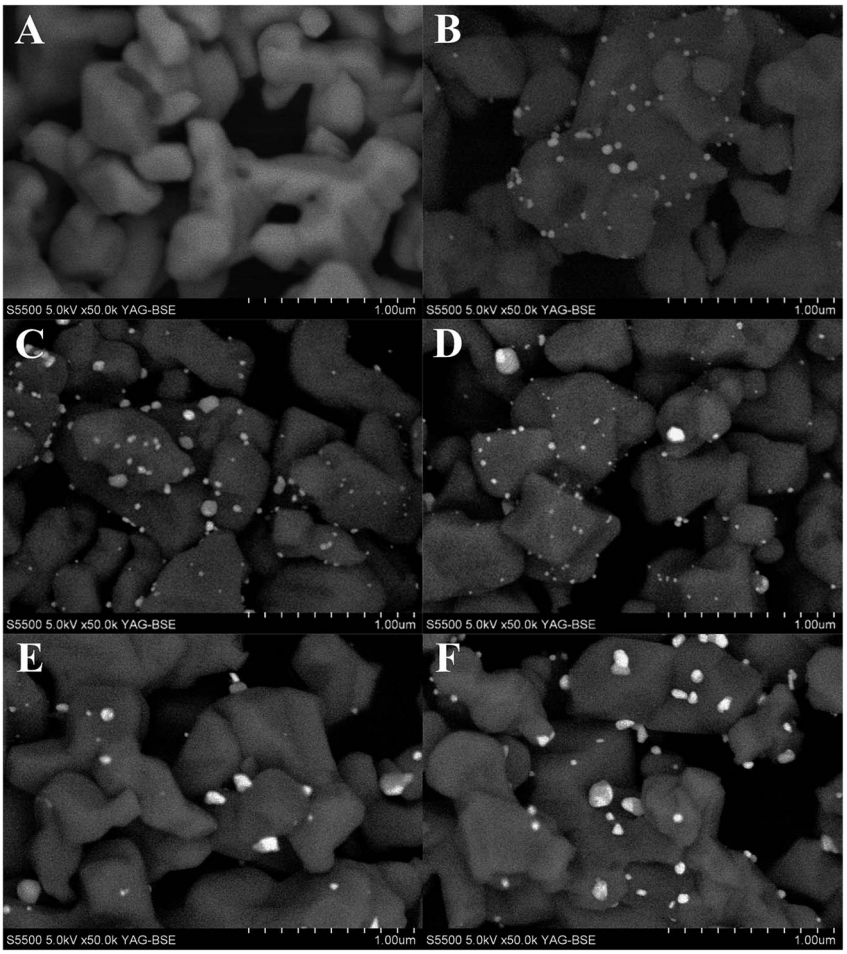

Fig. 2 SEM images of $Li_4Ti_5O_{12}$/Ag–Cu composites: (A) 0%, (B) 1%, (C) 2%, (D) 3%, (E) 4%, (F) 5% wt Ag–Cu.

respectively. The additional 2 peaks (signed as "+" in Fig. 1) at 38.11 and 44.28° correspond to the (111) and (200) planes of cubic structure of metallic silver (silver-3C, syn, cubic, *Fm3m*; ICDD-04-0783), respectively. The intensity of these two reflections increased with the increasing of Ag (and also Cu) content in all $Li_4Ti_5O_{12}$/Ag–Cu powders. Also, it should be pointed out, that the characteristic reflection line of Cu metallic at 43.29° (intensity of 100%, at (111) plane) matched to reflection line of LTO (43.28°; ICDD-04-0836). A systematic appearance of, mentioned above, two characteristics diffraction lines for metallic silver indicated that metallic Ag nanoparticles were successfully deposited on the surface of $Li_4Ti_5O_{12}$ (as we presented in our previous work).[76] It should be noted, that the process of surface modification of LTO grains using both silver and copper, nanoparticles in equal volume was reported in this work for the first time.

Lattice parameters of the lithium titanium oxide powders and their average crystallite sizes, calculated based on the XRD patterns shown in Fig. 1, are listed in Table 1. No significant change related to Ag–Cu presence was observed. In particular, for all samples, the average crystallites sizes of lithium–titanium oxide (as calculated from Scherrer formula, allowing for the instrumental line broadening) were in the range of 64 to 90 nm. The unit cell parameter of $Li_4Ti_5O_{12}$ powders with silver–copper nanoparticles calculated from the XRD data is consistent with the standard value (a_0 = 8.359 Å) of the ICDD PDF card.

The SEM images of $Li_4Ti_5O_{12}$/Ag–Cu composite powders are presented in Fig. 2. The Ag–Cu particles are visible on BSE images as bright particles located on lithium–titanium oxide substrate. It can be seen, that the Ag–Cu nanoparticles are below 100 nm in diameter and they are distributed on LTO surface relatively homogeneous. The SEM analysis did not show significant difference in Ag–Cu nanoparticles size for lower concentration (1–3%) and slight growth of the nanoparticles size for higher concentration (4–5%). In this case Ag–Cu nanoparticles with diameter above 100 nm can be observed.

STEM images confirms homogeneous distribution Ag–Cu particles on LTO surface (Fig. 3A and B). The differences in brightness intensity observed for different areas of Ag–Cu particles on HAADF-STEM images suggest elemental composition variability (Fig. 3B). It means that Ag–Cu particles composition is not homogenous. This observations were confirmed by EDS mapping results where silver content was found only in selected areas of Ag–Cu particles (Fig. 3C and D). The example of EDS spectrum taken from Ag–Cu particle area, indicated by the circle, is presented in Fig. 3E. The Cu-L and Ag-L lines, visible on the spectrum, confirm the presence of silver and copper elements in

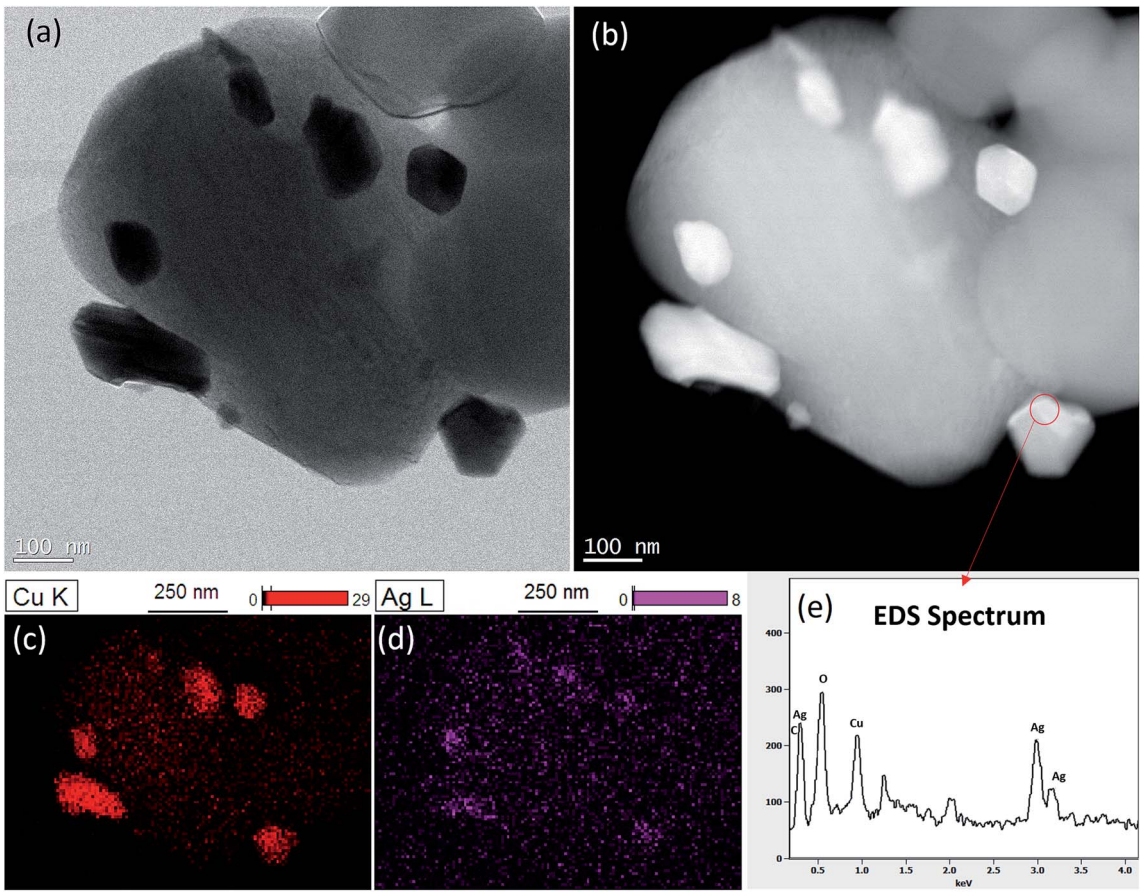

Fig. 3 STEM analysis of $Li_4Ti_5O_{12}$/5% Ag–Cu composite: (a) STEM, (b) HAADF-STEM, (c) Cu EDS mapping, (d) Ag EDS mapping, (e) EDS spectrum of the area circled in red.

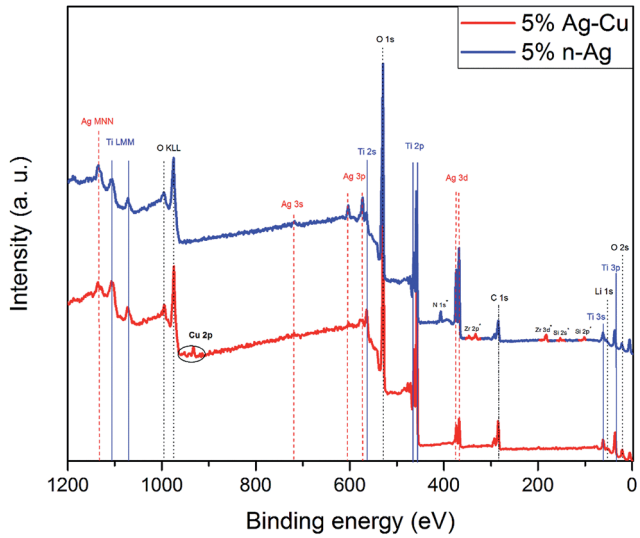

Fig. 4 XPS spectra of $Li_4Ti_5O_{12}$/5% Ag–Cu and $Li_4Ti_5O_{12}$/5% n-Ag composites.

one particle. Due to small volume of analyzed material, the signal is relatively weak, however the peaks of Ag and Cu are clearly visible. Other observed peaks are related to oxygen from $Li_4Ti_5O_{12}$ particle and sample contamination.

Fig. 4 represents the XPS wide scan spectrum of $Li_4Ti_5O_{12}$/5% Ag–Cu powder. It also includes wide scan of $Li_4Ti_5O_{12}$/5% n-Ag sample prepared by the same method and taken as a reference material.[78] The spectrum comprises several main peaks which correspond to titanium, oxygen and silver. Spectrum of $Li_4Ti_5O_{12}$/5% Ag–Cu also reveals the presence of copper in the sample: Cu $2p_{3/2}$ and Cu $2p_{1/2}$ peaks at 932.6 eV and 952.0 eV binding energies respectively. It can be also seen that $Li_4Ti_5O_{12}$/5% n-Ag powder is slightly contaminated by nitrogen (from $AgNO_3$ precursor) as well as zirconium and silicon (from ceramic mortar). The relative surface concentrations of main species present in both samples are listed in Table 2. Lithium–titanium oxide modified with 5% wt of silver nanoparticles reveals a significant amount of Ag at the surface of grains (21% wt). In comparison, surface concentration of silver in LTO sample modified with 2.5% wt of silver and 2.5% wt of copper is much lower (6% wt). It might indicates that silver in $Li_4Ti_5O_{12}$/5% Ag–Cu powder forms much larger grains of non-uniform distribution resulting in apparently lower concentration of Ag detected by XPS measurement. This statement is consisted with EDS mapping, which confirms high agglomeration of silver in $Li_4Ti_5O_{12}$/5% Ag–Cu sample. One can also recognize that surface copper content is 33% lower than silver even though bulk concentration of these specie is equal. It suggest that Ag localizes on the surface of Cu. This observations are consistent with EDS mapping. The presence of the most intense peaks (Ag 3d located at *ca.* 370 eV) at the XPS spectra is a clear evidence of silver existence at the surface of examined material. It can be seen, that spectra of $Li_4Ti_5O_{12}$/n-Ag sample consist of mainly Ag 3s, Ag 3p and Ag 3d photoelectron lines, although, due to decreasing of cross-section factor, the Ag 3s and Ag 3p peaks are of diminished intensity, in comparison with Ag 3d peak. In the case of $Li_4Ti_5O_{12}$/Ag–Cu sample, the surface concentration of silver is much lower, thus the Ag 3s and Ag 3p peaks are barely detected.

Table 2 Mass surface concentrations of titanium, oxygen, silver and copper elements in $Li_4Ti_5O_{12}$/5% n-Ag and $Li_4Ti_5O_{12}$/5% Ag–Cu composites

	Mass surface concentration [%]	
Element	5% n-Ag	5% Ag–Cu
Ti	35	48
O	44	44
Ag	21	6
Cu	—	2

3.2 Electrochemistry

3.2.1 Cyclability tests. Fig. 5 presents the initial discharge curves of pristine and Ag–Cu modified $Li_4Ti_5O_{12}$ during cyclability tests. All examined samples showed higher specific capacity than theoretical value of 175 mAh g^{-1} for lithium–titanium oxide during discharge at 0.1C rate. The extra charge is related to non-intercalation processes, involving electrode activation, reduction of trace water present in the electrolyte[28] or corrosion of copper current collector.[89,90] Fig. 6 and 7 presents the results of cyclability tests. Charge/discharge curves (Fig. 6) show that the insertion/extraction of Li^+ ions into/out of $Li_4Ti_5O_{12}$ framework occurs at a stable potential plateau of 1.58/1.54 V (*vs.* Li^+/Li^0) during charge and discharge, respectively. No other electrochemical processes were present in examined cells. Ag–Cu modification had no impact on specific capacity of $Li_4Ti_5O_{12}$ composite powders at 1C rate and all examined electrodes' specific capacity was in 160–162 mAh g^{-1} range. All studied powders also showed good cyclability (Fig. 7),

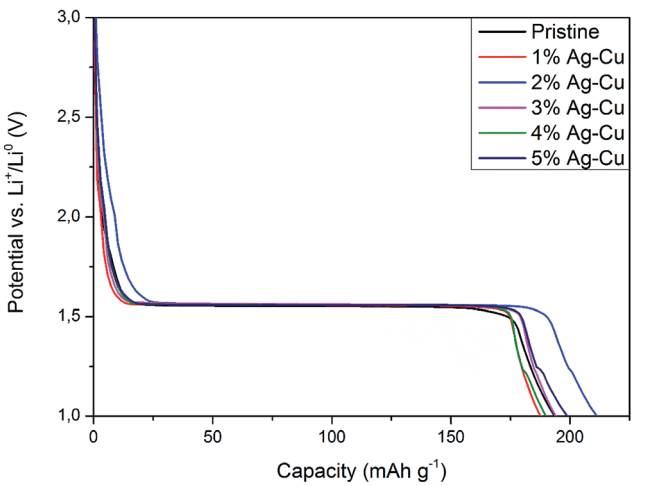

Fig. 5 Initial discharge curves of $Li_4Ti_5O_{12}$/Ag–Cu composites during cyclability tests.

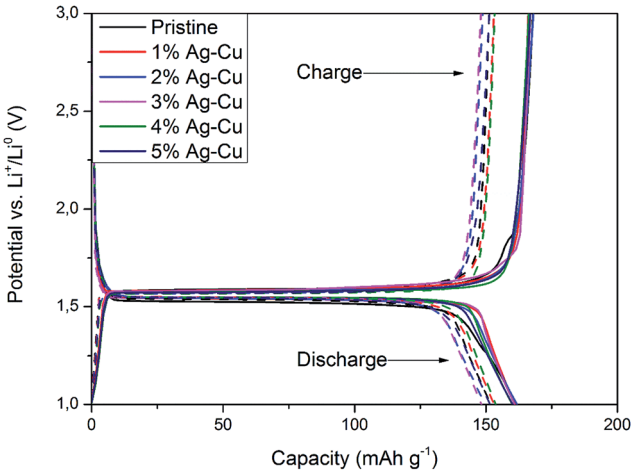

Fig. 6 Charge/discharge curves for $Li_4Ti_5O_{12}$/Ag–Cu composites during cyclability tests: solid line – 1st cycle, dashed line – 50th cycle.

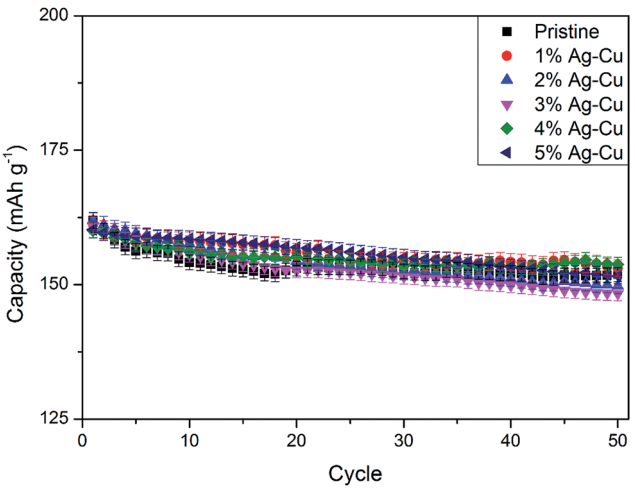

Fig. 7 Cyclability of $Li_4Ti_5O_{12}$/Ag–Cu composites.

maintaining between 92 and 96% specific capacity retention after 50 charge/discharge cycles. No dependency between cyclability of $Li_4Ti_5O_{12}$ and the amount of mixed Ag–Cu modification in examined powders was found. The results of cyclability tests were also listed in Table 3.

3.2.2 High-rate tests. Fig. 8 shows the initial discharge curves of $Li_4Ti_5O_{12}$/Ag–Cu composites during high-rate tests. Similar to cyclability tests, the examined cells showed higher specific capacity than theoretical value for LTO, suggesting other, non-faradaic processes present during the initial discharge. The results of high-rate tests are presented on Fig. 9, 10 and in Table 4. Also in this case, the examined electrodes' specific capacity at 1C rate was in 160–162 mAh g^{-1} range and no relationship between specific capacity at 1C rate and the amount of Ag–Cu modification was found. However, after raising the current rate, $Li_4Ti_5O_{12}$/Ag–Cu powders behavior began to differ from each other. At 10C rate, every modified sample reveals higher specific capacity than pristine one, reaching 101.1 ± 1.0 mAh g^{-1} for $Li_4Ti_5O_{12}$/5% Ag–Cu composite and retaining 63.13 ± 0.01% of specific capacity at 1C rate. On the other hand, the pristine sample showed only 82.0 ± 0.7 mAh g^{-1} of specific capacity and retained 50.59 ± 0.01% of its 1C rate specific capacity while discharged at 10C current rate. From Fig. 10, one can also see, that every modified sample has higher operating potential than pristine powder. All the above suggest better reaction kinetics and lower electrodes polarization for $Li_4Ti_5O_{12}$/Ag–Cu compounds. In order to get a better insight on the reasons behind enhanced electrochemical properties of Ag–Cu modified composite powders we conducted CV and EIS experiments.

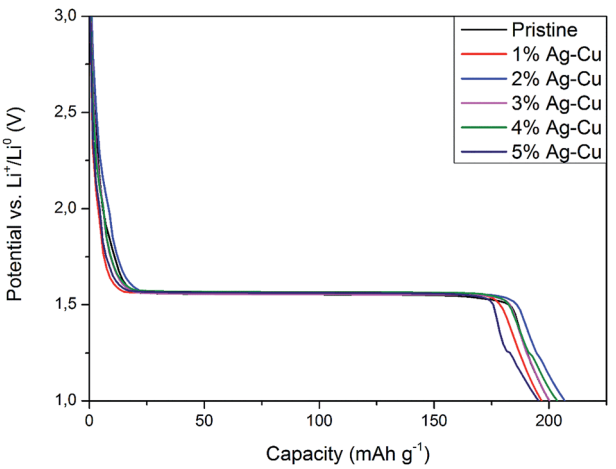

Fig. 8 Initial discharge curves of $Li_4Ti_5O_{12}$/Ag–Cu composites during high-rate tests.

Table 3 Results of cyclability CP tests of $Li_4Ti_5O_{12}$/Ag–Cu composites

Material	Electrode loading [mg cm^{-2}] (±0.02 mg cm^{-2})	Initial discharge capacity [mAh g^{-1}]	1st discharge capacity [mAh g^{-1}]	50th discharge capacity [mAh g^{-1}]	1st charge capacity [mAh g^{-1}]	50th charge capacity [mAh g^{-1}]	Capacity retained after 50th cycle [%] (±0.01%)
Pristine	2.19	193.5 ± 1.7	161.9 ± 1.4	151.9 ± 1.4	167.9 ± 1.5	151.2 ± 1.3	93.84
1% Ag–Cu	1.92	187.6 ± 1.9	161.1 ± 1.6	153.1 ± 1.6	166.1 ± 1.7	153.0 ± 1.6	94.99
2% Ag–Cu	2.05	211.2 ± 2.0	161.9 ± 1.6	149.7 ± 1.4	168.0 ± 1.6	148.8 ± 1.4	92.50
3% Ag–Cu	2.14	194.0 ± 1.8	161.0 ± 1.5	148.3 ± 1.4	166.9 ± 1.5	148.1 ± 1.4	92.16
4% Ag–Cu	2.29	189.9 ± 1.6	160.0 ± 1.4	153.8 ± 1.3	166.3 ± 1.4	153.3 ± 1.3	96.08
5% Ag–Cu	2.13	198.9 ± 1.8	160.2 ± 1.5	151.6 ± 1.4	166.9 ± 1.5	151.3 ± 1.4	94.62

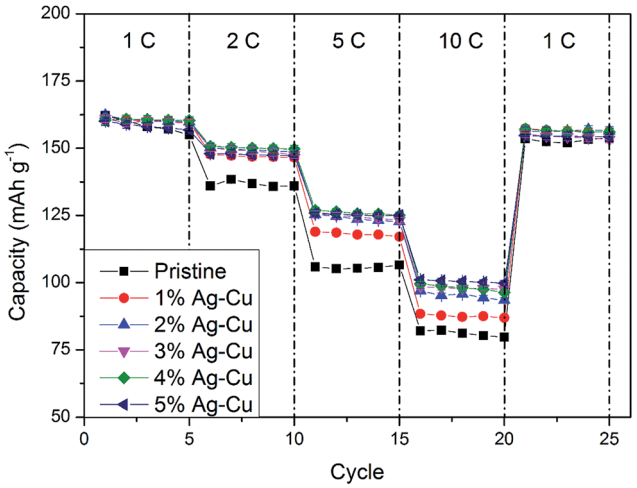

Fig. 9 Rate capability of $Li_4Ti_5O_{12}$/Ag–Cu composites.

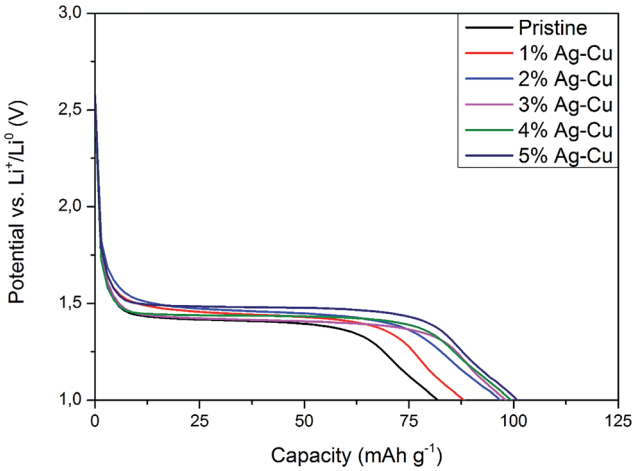

Fig. 10 Discharge curves of $Li_4Ti_5O_{12}$/Ag–Cu composites at 10C rate.

3.2.3 Cyclic voltammetry. Fig. 11 presents CV curves of pristine and Ag–Cu modified $Li_4Ti_5O_{12}$. One can see, that the peaks originated only from oxidation and reduction reactions of $Li_4Ti_5O_{12}$ and no other signals are visible. With increasing amount of Ag–Cu in analyzed composite powders, one can see slight changes in CV curves resulting in narrowed peak shape. This phenomenon is a result of better reaction kinetics and lower electrode's resistance after surface modification.[91] Increasing the scan rate resulted in higher peak currents and increase in oxidation–reduction peak separation (caused mainly by electrode's polarization). The linear trend of relationship between current intensity and square root of scan rate had been present in all examined samples (Fig. 12), which suggests a diffusion-controlled mechanism of oxidation/reduction reactions. According to Randles–Sevcik equation for a reversible electrochemical process, $I_p(v^{1/2})$ relationship can be described as:[92,93]

$$I_p = 0.4463\left(\frac{n^3F^3}{RT}vD\right)^{1/2}AC, \quad (3)$$

in which A is electrode's electrochemically active surface area (cm^2), v is scan rate ($V\ s^{-1}$), n is number of electrons involved during the electrochemical process, F is Faraday's constant ($C\ mol^{-1}$), R is gas constant ($J\ (mol\ K)^{-1}$), T is absolute temperature (K), C is molar concentration of lithium ions in $Li_4Ti_5O_{12}$ crystal ($mol\ cm^{-3}$) and D is chemical diffusion coefficient of lithium ions inside $Li_4Ti_5O_{12}$ matrix ($cm^2\ s^{-1}$), described as:

$$D = \frac{2D_{Li^+}D_{e^-}}{D_{Li^+} + D_{e^-}}, \quad (4)$$

and dependent on both Li^+ ion and electron diffusion in the host matrix.[91] By using the eqn (3) and equations obtained from linear functions of $I_p(v^{1/2})$, we calculated Li^+ ion chemical diffusion coefficient values for oxidation and reduction reactions of $Li_4Ti_5O_{12}$/Ag–Cu powders (Fig. 13) and listed them in Table 5. Because of the two-phase mechanism of LTO intercalation/deintercalation reaction and poor Li^+ ionic conductivity of fully reduced compound ($Li_7Ti_5O_{12}$ of rock-salt structure),[94] Li^+ ion transport across lithium–titanium oxide matrix is faster during oxidation reaction, which corresponds to higher Li^+ chemical diffusion coefficient values for oxidation processes.

Modification of $Li_4Ti_5O_{12}$ surface resulted in an increase in chemical diffusion coefficient values for every modified sample – from $(4.31 \pm 0.11) \times 10^{-10}$ and $(1.88 \pm 0.08) \times 10^{-10}\ cm^2\ s^{-1}$ for pristine LTO oxidation and reduction processes to $(9.41 \pm 0.73) \times 10^{-10}$ and $(4.33 \pm 0.13) \times 10^{-10}\ cm^2\ s^{-1}$ for $Li_4Ti_5O_{12}$/5% Ag–Cu oxidation and reduction reactions. Furthermore, with every increase of Ag–Cu amount in examined powders the values of D increased. There is no saturation in chemical

Table 4 Results of high-rate CP tests of $Li_4Ti_5O_{12}$/Ag–Cu composites

Material	Electrode loading [mg cm^{-2}] ($\pm$0.02 mg cm^{-2})	Initial discharge capacity [mAh g^{-1}]	1C discharge capacity [mAh g^{-1}]	2C discharge capacity [mAh g^{-1}]	5C discharge capacity [mAh g^{-1}]	10C discharge capacity [mAh g^{-1}]	Capacity retained at 10C [%] ($\pm$0.01%)
Pristine	2.16	200.3 ± 1.8	162.1 ± 1.5	136.0 ± 1.2	105.9 ± 1.0	82.0 ± 0.7	50.59
1% Ag–Cu	2.27	196.8 ± 1.7	160.9 ± 1.4	147.8 ± 1.3	118.9 ± 1.0	88.4 ± 0.8	54.95
2% Ag–Cu	1.99	206.9 ± 2.0	162.3 ± 1.6	150.3 ± 1.5	125.3 ± 1.2	97.0 ± 1.0	59.76
3% Ag–Cu	2.28	200.2 ± 1.7	161.1 ± 1.4	150.1 ± 1.3	125.7 ± 1.1	98.4 ± 0.8	61.12
4% Ag–Cu	2.15	203.6 ± 1.9	160.5 ± 1.5	150.8 ± 1.4	126.9 ± 1.2	99.7 ± 0.9	62.11
5% Ag–Cu	1.98	195.4 ± 1.9	160.1 ± 1.6	148.0 ± 1.5	125.9 ± 1.2	101.1 ± 1.0	63.13

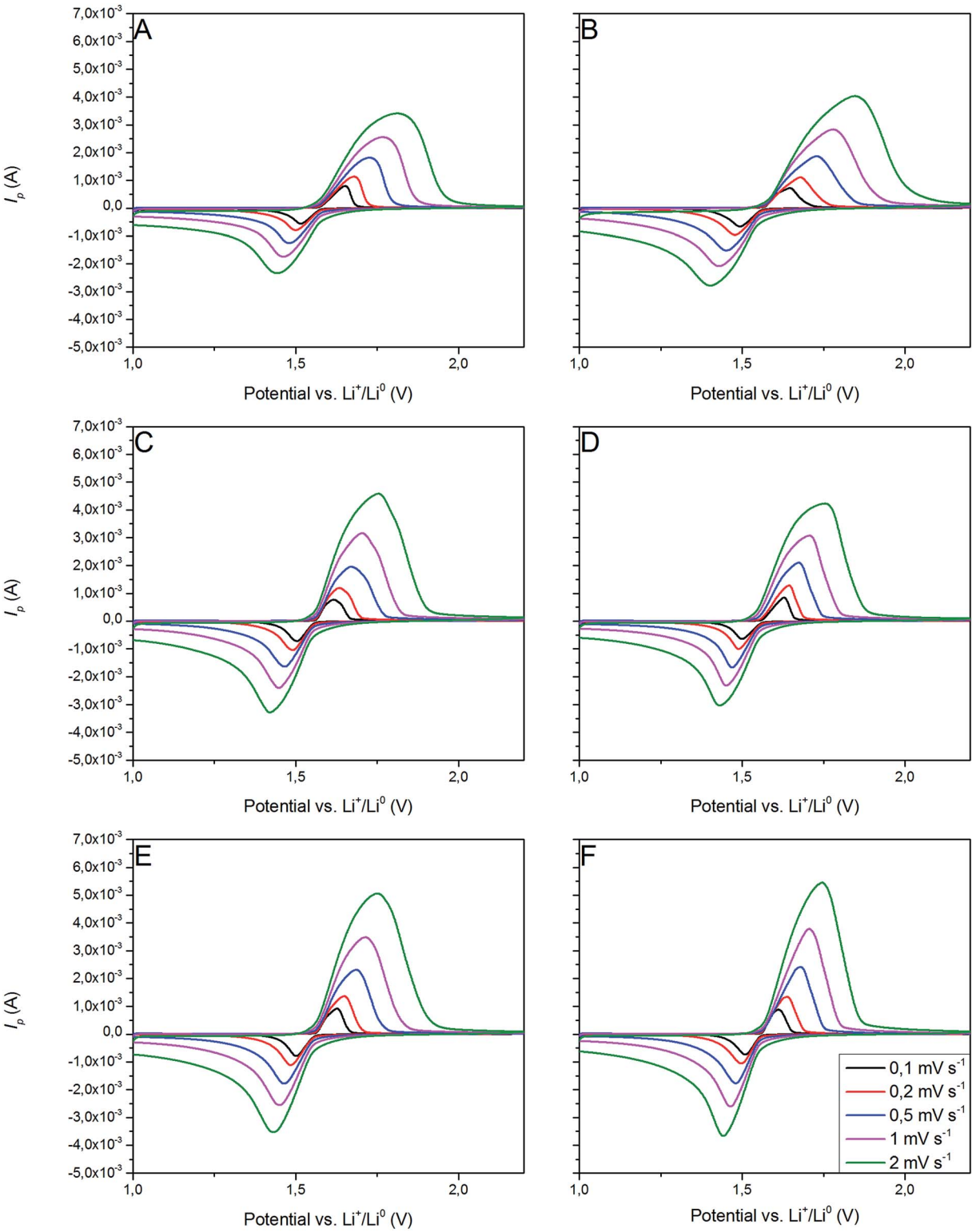

Fig. 11 CV curves of $Li_4Ti_5O_{12}$/Ag–Cu composites: (A) 0%, (B) 1%, (C) 2%, (D) 3%, (E) 4%, (F) 5% wt Ag–Cu.

diffusion coefficients occurring while increasing the amount of Ag–Cu modification, which suggest that the lithium–titanium oxide's particles are not fully covered with silver and copper even at 5% wt of Ag–Cu. These findings are in good agreement with SEM, XPS, galvanostatic measurements and with our previous studies about $Li_4Ti_5O_{12}$/n-Ag composites[78,79] and can be explained by increase in electrode's active surface area and the amount of active centers capable of insertion/extraction reaction of Li^+ ions into/out of $Li_4Ti_5O_{12}$ framework[79] but, as the LTO's surface is not covered completely by silver–copper

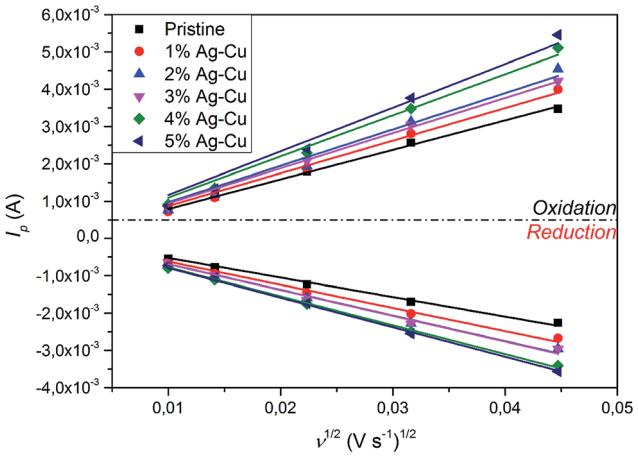

Fig. 12 $I_p(v^{-1/2})$ relationship acquired from CV curves of $Li_4Ti_5O_{12}$/Ag–Cu composites.

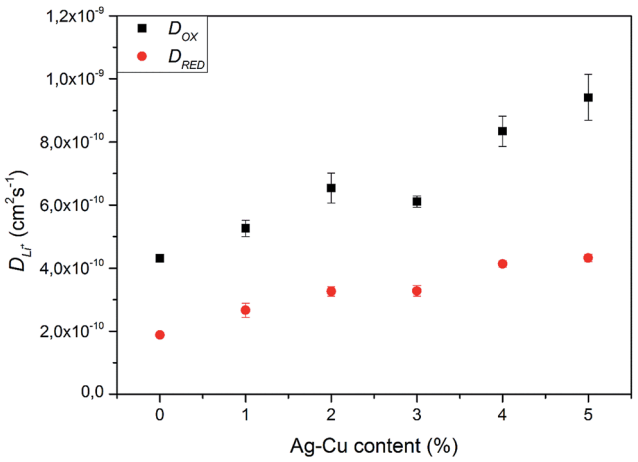

Fig. 13 Li^+ chemical diffusion coefficient values calculated from CV experiments of $Li_4Ti_5O_{12}$/Ag–Cu composites.

particles, the electrochemical performance of $Li_4Ti_5O_{12}$/Ag–Cu composites is not as good as in the case of $Li_4Ti_5O_{12}$/n-Ag[78] due to lower electrochemically active surface area of examined composites than in our previous studies.[79]

3.2.4 Electrochemical impedance spectroscopy. Fig. 14 presents the complex plane plots of pristine and Ag–Cu

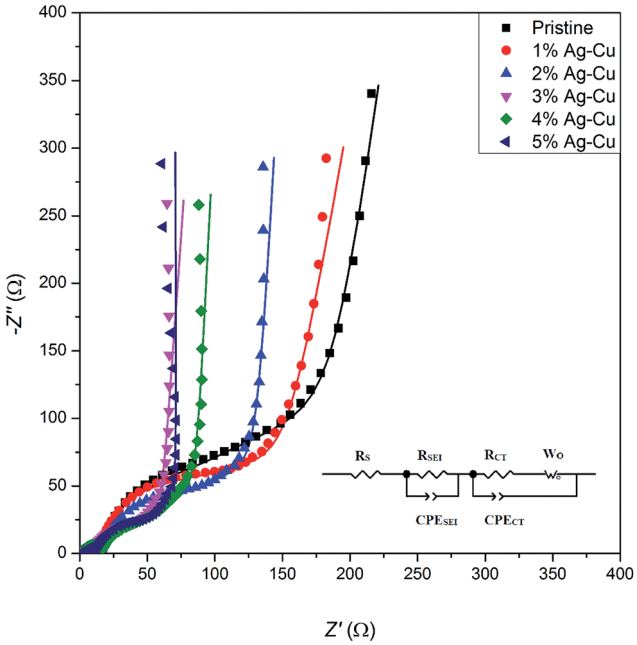

Fig. 14 Complex plane plots of $Li_4Ti_5O_{12}$/Ag–Cu composites. Inset shows the equivalent circuit used for data fitting.

modified lithium–titanium oxide. The equivalent circuit used for data fitting is presented in the inset of Fig. 14. In the mentioned circuit, R_S corresponds to ohmic resistance (intersection with Z' axis at high frequency), R_{SEI} is the resistance of passivation film on electrode's surface (depressed semicircle at high frequencies), R_{CT} is the charge-transfer resistance through electrode|electrolyte interface (depressed semicircle at medium frequencies), CPE elements correspond to capacitance of Li^+ transport through SEI layer and electrode's surface and W_O is a Warburg resistance linked to a long-range diffusion of Li^+ ions inside lithium–titanium oxide crystal (inclined line at low frequencies).[4,54–56,75] The results obtained through data fitting are listed in Table 6. One can see, that Ag–Cu modification resulted in lower R_{CT} values of $Li_4Ti_5O_{12}$/Ag–Cu composites, suggesting faster reaction kinetics and increased conductivity of synthesized composite powders. After reaching 3% wt of Ag–Cu modification the charge-transfer resistance stabilizes in the range of 17–25 Ω, which is *ca.* 30 Ω lower than for pristine sample.

Table 5 Li^+ chemical diffusion coefficient values calculated from CV experiments of $Li_4Ti_5O_{12}$/Ag–Cu composites

Material	Electrode loading [mg cm^{-2}] (±0.02 mg cm^{-2})	D_{OX} [cm^2 s^{-1}]	D_{RED} [cm^2 s^{-1}]
Pristine	2.13	$(4.31 \pm 0.11) \times 10^{-10}$	$(1.88 \pm 0.08) \times 10^{-10}$
1% Ag–Cu	2.35	$(5.26 \pm 0.26) \times 10^{-10}$	$(2.66 \pm 0.22) \times 10^{-10}$
2% Ag–Cu	2.08	$(6.54 \pm 0.48) \times 10^{-10}$	$(3.26 \pm 0.15) \times 10^{-10}$
3% Ag–Cu	2.26	$(6.11 \pm 0.18) \times 10^{-10}$	$(3.28 \pm 0.17) \times 10^{-10}$
4% Ag–Cu	2.19	$(8.34 \pm 0.48) \times 10^{-10}$	$(4.14 \pm 0.10) \times 10^{-10}$
5% Ag–Cu	1.98	$(9.41 \pm 0.73) \times 10^{-10}$	$(4.33 \pm 0.13) \times 10^{-10}$

Table 6 Data acquired after fitting and analysis of EIS spectra of $Li_4Ti_5O_{12}$/Ag–Cu composites

Material	Electrode loading [mg cm^{-2}] (±0.02 mg cm^{-2})	R_S [Ω]	R_{SEI} [Ω]	R_{CT} [Ω]	D_{EIS} [cm^2 s^{-1}]
Pristine	2.13	2.82 ± 0.05	14.26 ± 0.19	58.78 ± 2.60	(6.20 ± 0.69) × 10^{-14}
1% Ag–Cu	2.25	3.47 ± 0.03	12.67 ± 0.19	62.81 ± 2.60	(1.12 ± 0.11) × 10^{-13}
2% Ag–Cu	2.08	3.08 ± 0.03	14.52 ± 0.18	50.57 ± 2.02	(1.31 ± 0.14) × 10^{-13}
3% Ag–Cu	2.23	2.36 ± 0.02	6.57 ± 0.14	24.48 ± 1.85	(1.64 ± 0.16) × 10^{-13}
4% Ag–Cu	2.19	2.34 ± 0.06	16.09 ± 0.21	17.27 ± 1.24	(1.98 ± 0.10) × 10^{-13}
5% Ag–Cu	1.91	3.13 ± 0.04	9.72 ± 0.13	22.03 ± 1.20	(2.53 ± 0.27) × 10^{-13}

We calculated Li^+ ion chemical diffusion coefficient from EIS data by using the equation:[13,15,25,26,34,47]

$$D = \frac{1}{2}\left(\frac{RT}{An^2F^2C\sigma}\right)^2, \quad (5)$$

in which σ is a Warburg coefficient (Ω s^{-1}), corresponding to a slope of $Z'(\omega^{-1/2})$ function, described by equation:

$$Z' = \text{const} + \sigma\omega^{-1/2}, \quad (6)$$

and fulfilled for the frequency range in which the EIS spectrum is inclined to Z' axis at 45° (Fig. 15). The rest of the symbols have the same meaning as in eqn (3). The acquired D values are presented on Fig. 16 and listed in Table 6. The obtained lithium ion chemical diffusion coefficient values show similar trend with increasing Ag–Cu content in $Li_4Ti_5O_{12}$/Ag–Cu composite as in the case of CV experiments. One can see an increase in D values with increasing amount of Ag–Cu modification – from (6.20 ± 0.69) × 10^{-14} cm^2 s^{-1} for pristine powder to (2.53 ± 0.27) × 10^{-13} cm^2 s^{-1} for $Li_4Ti_5O_{12}$/Ag–Cu composite. EIS results are also in good agreement with galvanostatic tests and with our previous studies about $Li_4Ti_5O_{12}$/n-Ag compounds[78,79] and can be explained by enhancing the surface conductivity of $Li_4Ti_5O_{12}$, enhancing its electrochemically active surface area and providing more active centers for intercalation/deintercalation reactions to take place.[79] Also in this case, the saturation of D values is not present, which suggest not fully covered crystals of $Li_4Ti_5O_{12}$ by Ag–Cu modification, as seen on SEM and XPS results, and lower electrochemically active surface area than in our previous studies about $Li_4Ti_5O_{12}$/n-Ag compounds.[79]

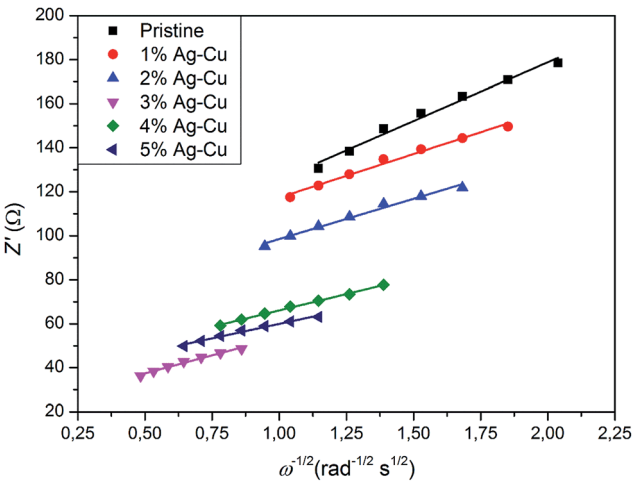

Fig. 15 $Z'(\omega^{-1/2})$ relationship acquired from EIS experiments of $Li_4Ti_5O_{12}$/Ag–Cu composites.

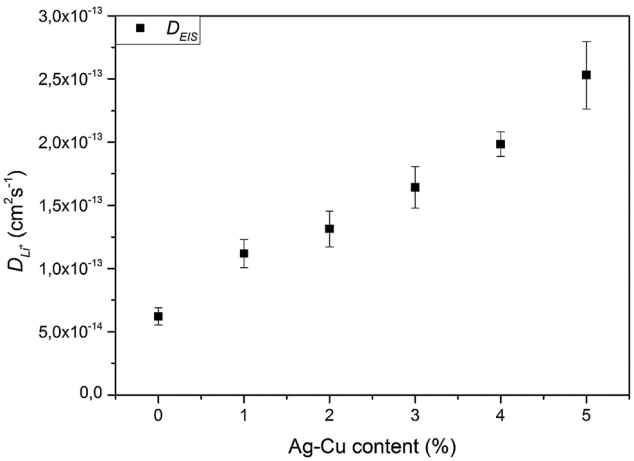

Fig. 16 Li^+ chemical diffusion coefficient values calculated from EIS spectra of $Li_4Ti_5O_{12}$/Ag–Cu composites.

4. Conclusions

We successfully synthesized lithium–titanium oxide and modified its surface with Ag–Cu metals. The XRD and SEM experiments showed a presence of metallic nanoparticles, 100 nm in diameter, in examined powders. XPS experiments revealed lower surface concentration of Ag–Cu particles than in the case of $Li_4Ti_5O_{12}$/5% n-Ag composite. Galvanostatic charge/discharge evaluation of studied materials showed enhanced electrochemical properties of $Li_4Ti_5O_{12}$ powders after Ag–Cu modification, namely *ca.* 12.5% increase in specific capacity retention at 10C current rate and *ca.* 19 mAh g^{-1} increase in specific capacity at 10C current rate were observed. Furthermore, CV and EIS experiments showed an increase in Li^+ chemical diffusion coefficient values with increasing amount of Ag–Cu present in $Li_4Ti_5O_{12}$/Ag–Cu composites and decrease in examined powders impedance and charge-transfer resistance after Ag–Cu surface modification.

Enhanced electrochemical properties of $Li_4Ti_5O_{12}$/Ag–Cu composites are an effect of $Li_4Ti_5O_{12}$ surface activation through

contact with conductive particles. That mechanism was more thoroughly explained in our previous work.[79] This research is in very good agreement with our previous studies about $Li_4Ti_5O_{12}$/n-Ag composites[78,79] and gives insight on the influence of conductive particles morphology and surface coverage on electrochemistry of electrode materials. It also further confirms a positive effect of conductive nanoparticles deposition on electrode's material surface on its electrochemical properties for next generation of lithium-ion batteries. Additional studies are currently in progress, involving $Li_4Ti_5O_{12}$ modified only with copper element and controlling the morphology of metal deposits by using reducing and complexing agents.

Conflicts of interest

There are no conflicts to declare.

Acknowledgements

This work was supported by The Polish National Centre of Research and Development through the research grant PBS1/A1/4/2012 and by The Polish National Centre of Science through the research grant UMO-2014/15/B/ST5/02118.

References

1 S. Panero, P. Reale, F. Ronci, B. Scrosati, P. Perfetti and V. R. Albertini, Refined, in-situ EDXD structural analysis of the $Li[Li_{1/3}Ti_{5/3}]O_4$ electrode under lithium insertion-extraction, *Phys. Chem. Chem. Phys.*, 2001, **3**, 845.

2 T. Ohzuku, A. Ueda and N. Yamamoto, Zero-Strain Insertion Material of $Li[Li_{1/3}Ti_{5/3}]O_4$ for Rechargeable Lithium Cells, *J. Electrochem. Soc.*, 1995, **142**, 1431.

3 T. Nordh, R. Younesi, D. Brandell and K. Edström, Depth profiling the solid electrolyte interface on lithium titanate ($Li_4Ti_5O_{12}$) using synchrotron-based photoelectron spectroscopy, *J. Power Sources*, 2015, **294**, 173.

4 R. Dedryvère, D. Foix, S. Franger, S. Patoux, L. Daniel and D. Gonbeau, Electrode/Electrolyte Interface Reactivity in High-Voltage Spinel $LiMn_{1.6}Ni_{0.4}O_4/Li_4Ti_5O_{12}$ Lithium-Ion Battery, *J. Phys. Chem. C*, 2010, **114**, 10999.

5 H. Ge, N. Li, D. Li, C. Dai and D. Wang, Study on the Theoretical Capacity of Spinel Lithium Titanate Induced by Low-Potential Intercalation, *J. Phys. Chem. C*, 2009, **113**, 6324.

6 C. Y. Ouyang, Z. Y. Zhong and M. S. Lei, Ab initio studies of structural and electronic properties of $Li_4Ti_5O_{12}$ spinel, *Electrochem. Commun.*, 2007, **9**, 1107.

7 T.-F. Yi, L.-J. Jiang, J. Shu, C.-B. Yue, R.-S. Zhu and H.-B. Qiao, Recent development and application of $Li_4Ti_5O_{12}$ as anode material of lithium ion battery, *J. Phys. Chem. Solids*, 2010, **71**, 1236.

8 T.-F. Yi, S.-Y. Yang and Y. Xie, Recent advances of $Li_4Ti_5O_{12}$ as a promising next generation anode material for high power lithium-ion batteries, *J. Mater. Chem. A*, 2015, **3**, 5750.

9 W. Ojczyk, J. Marzec, K. Swierczek, W. Zajac, M. Molenda, R. Dziembaj and J. Molenda, Studies of selected synthesis procedures of the conducting $LiFePO_4$-based composite cathode materials for Li-ion batteries, *J. Power Sources*, 2007, **173**, 700.

10 G. Xu, Z. Liu, C. Zhang, G. Cui and L. Chen, Strategies for improving the cyclability and thermos-stability of $LiMn_2O_4$-based batteries at elevated temperatures, *J. Mater. Chem. A*, 2015, **3**, 4092.

11 D. Ziolkowska, K. Korona, B. Hamankiewicz, S.-H. Wu, M.-S. Chen, J. B. Jasinski, M. Kaminska and A. Czerwinski, The role of SnO_2 surface coating on the electrochemical performance of $LiFePO_4$ cathode materials, *Electrochim. Acta*, 2013, **108**, 532.

12 M. Michalska, B. Hamankiewicz, D. Ziolkowska, M. Krajewski, L. Lipinska, M. Andrzejczuk and A. Czerwinski, Influence of $LiMn_2O_4$ modification with CeO_2 on electrode performance, *Electrochim. Acta*, 2014, **136**, 286.

13 B. Hamankiewicz, M. Michalska, M. Krajewski, D. Ziolkowska, L. Lipińska, K. Korona, M. Kaminska and A. Czerwinski, The effect of electrode thickness on electrochemical performance of $LiMn_2O_4$ cathode synthesized by modified sol-gel method, *Solid State Ionics*, 2014, **262**, 9.

14 W. Liu, J. Zhang, Q. Wang, X. Xie, Y. Lou and B. Xia, The effects of Li_2CO_3 particle size on the properties of lithium titanate as anode material for lithium-ion batteries, *Ionics*, 2014, **20**, 1553.

15 T.-F. Yi, S.-Y. Yang, M. Tao, Y. Xie, Y.-R. Zhu and R.-S. Zhu, Synthesis and application of a novel $Li_4Ti_5O_{12}$ composite as anode material with enhanced fast charge-discharge performance for lithium-ion battery, *Electrochim. Acta*, 2014, **134**, 377.

16 X. Li, H. Hu, S. Huang, G. Yu, L. Gao, H. Liu and Y. Yu, Nano-sized $Li_4Ti_5O_{12}$ anode material with excellent performance prepared by solid state reaction: The effect of precursor size and morphology, *Electrochim. Acta*, 2013, **112**, 356.

17 W. Liu, J. Zhang, Q. Wang, X. Xie, Y. Lou, X. Han and B. Xia, Microsized TiO_2 activated by high-energy ball milling as starting material for the preparation of $Li_4Ti_5O_{12}$ anode material, *Powder Technol.*, 2013, **247**, 204.

18 M. Michalska, M. Krajewski, D. Ziolkowska, B. Hamankiewicz, M. Andrzejczuk, L. Lipinska, K. P. Korona and A. Czerwinski, Influence of milling time in solid-state synthesis on structure, morphology and electrochemical properties of $Li_4Ti_5O_{12}$ of spinel structure, *Powder Technol.*, 2014, **266**, 372.

19 G. Luo, J. He, X. Song, X. Huang, X. Yu, Y. Fang and D. Chen, Bamboo carbon assisted sol-gel synthesis of $Li_4Ti_5O_{12}$ anode material with enhanced electrochemical activity for lithium ion battery, *J. Alloys Compd.*, 2015, **621**, 268.

20 Y.-J. Hao, Q.-Y. Lai, J.-Z. Lua, D.-Q. Liu and X.-Y. Ji, Influence of various complex agents on electrochemical property of $Li_4Ti_5O_{12}$ anode material, *J. Alloys Compd.*, 2007, **439**, 330.

21 R. B. Khomane, A. S. Prakash, K. Ramesha and M. Sathiya, CTAB-assisted sol-gel synthesis of $Li_4Ti_5O_{12}$ and its electrochemical performance as anode material for Li-ion batteries, *Mater. Res. Bull.*, 2011, **46**, 1139.

22 N. Zhang, Z. Liu, T. Yang, C. Liao, Z. Wang and K. Sun, Facile preparation of nanocrystalline $Li_4Ti_5O_{12}$ and its high electrochemical performance as anode material for lithium-ion batteries, *Electrochem. Commun.*, 2011, **13**, 654.

23 C. Jiang, Y. Zhou, I. Honma, T. Kudo and H. Zhou, Preparation and rate capability of $Li_4Ti_5O_{12}$ hollow-sphere anode material, *J. Power Sources*, 2007, **166**, 514.

24 Q. Zhou, L. Liu, H. Guo, R. Xu, J. Tan, Z. Yan, Z. Huang, H. Shu, X. Yang and X. Wang, Synthesis of nanosheets-assembled lithium titanate hollow microspheres and their application to lithium ion battery anodes, *Electrochim. Acta*, 2015, **151**, 502.

25 T.-F. Yi, S.-Y. Yang, Y.-R. Zhu, M.-F. Ye, Y. Xie and R.-S. Zhu, Enhanced rate performance of $Li_4Ti_5O_{12}$ anode material by ethanol-assisted hydrothermal synthesis for lithium-ion battery, *Ceram. Int.*, 2014, **40**, 9853.

26 W. Liu, D. Shao, G. Luo, Q. Gao, G. Yan, J. He, D. Chen, X. Yu and Y. Fang, Mesoporous Spinel $Li_4Ti_5O_{12}$ Nanoparticles for High Rate Lithium-ion Battery Anodes, *Electrochim. Acta*, 2014, **133**, 578.

27 Y. Li, G. L. Pan, J. W. Liu and X. P. Gao, Preparation of $Li_4Ti_5O_{12}$ Nanorods as Anode Materials for Lithium-Ion Batteries, *J. Electrochem. Soc.*, 2009, **156**, A495.

28 Y. Tang, L. Yang, S. Fang and Z. Qiu, $Li_4Ti_5O_{12}$ hollow microspheres assembled by nanosheets as an anode material for high-rate lithium ion batteries, *Electrochim. Acta*, 2009, **54**, 6244.

29 T. Yuan, R. Cai, K. Wang, R. Ran, S. Liu and Z. Shao, Combustion synthesis of high-performance $Li_4Ti_5O_{12}$ for secondary Li-ion battery, *Ceram. Int.*, 2009, **35**, 1757.

30 J. Wang, H. Zhao, Y. Wen, J. Xie, Q. Xia, T. Zhang, Z. Zeng and X. Du, High performance $Li_4Ti_5O_{12}$ material as anode for lithium-ion batteries, *Electrochim. Acta*, 2013, **113**, 679.

31 A. S. Prakash, P. Manikandan, K. Ramesha, M. Sathiya, J.-M. Tarascon and A. K. Shukla, Solution-Combustion Synthesized Nanocrystalline $Li_4Ti_5O_{12}$ As High-Rate Performance Li-Ion Battery Anode, *Chem. Mater.*, 2010, **22**, 2857.

32 J. Li, Y.-L. Jin, X.-G. Zhang and H. Yang, Microwave solid-state synthesis of spinel $Li_4Ti_5O_{12}$ nanocrystallites as anode material for lithium-ion batteries, *Solid State Ionics*, 2007, **178**, 1590.

33 L. H. Yang, C. Dong and J. Guo, Hybrid microwave synthesis and characterization of the compounds in the Li-Ti-O system, *J. Power Sources*, 2008, **175**, 575.

34 S.-L. Chou, J.-Z. Wang, H.-K. Liu and S.-X. Dou, Rapid Synthesis of $Li_4Ti_5O_{12}$ Microspheres as Anode Materials and Its Binder Effect for Lithium-Ion Battery, *J. Phys. Chem. C*, 2011, **115**, 16220.

35 S. H. Ju and Y. C. Kang, Effects of types of drying control chemical additives on the morphologies and electrochemical properties of $Li_4Ti_5O_{12}$ anode powders prepared by spray pyrolysis, *J. Alloys Compd.*, 2010, **506**, 913.

36 X. Zhang, H. Xu, Y. Zhao, G. Zhu and A. Yu, A facile one-step spray pyrolysis method to synthesize spherical $Li_4Ti_5O_{12}$ for lithium-ion battery, *Mater. Lett.*, 2014, **129**, 101.

37 V. Miikkulainen, O. Nilsen, M. Laitinen, T. Sajavaara and H. Fjellvåg, Atomic layer deposition of $Li_xTi_yO_z$ thin films, *RSC Adv.*, 2013, **3**, 7537.

38 S. Ji, J. Zhang, W. Wang, Y. Huang, Z. Feng, Z. Zhang and Z. Tang, Preparation and effects of Mg-doping on the electrochemical properties of spinel $Li_4Ti_5O_{12}$ as anode material for lithium ion battery, *Mater. Chem. Phys.*, 2010, **123**, 510.

39 W. Wang, B. Jiang, W. Xiong, Z. Wang and S. Jiao, A nanoparticle Mg-doped $Li_4Ti_5O_{12}$ for high rate lithium-ion batteries, *Electrochim. Acta*, 2013, **114**, 198.

40 C. Lin, M. O. Lai, L. Lu, H. Zhou and Y. Xin, Structure and high rate performance of Ni^{2+} doped $Li_4Ti_5O_{12}$ for lithium ion battery, *J. Power Sources*, 2013, **244**, 272.

41 S. Huang, Z. Wen, Z. Gu and X. Zhu, Preparation and cycling performance of Al^{3+} and F^- co-substituted compounds $Li_4Al_xTi_{5-x}F_yO_{12-y}$, *Electrochim. Acta*, 2005, **50**, 4057.

42 J. S. Park, S.-H. Baek, Y.-I. Jeong, B.-Y. Noh and J. H. Kim, Effects of a dopant on the electrochemical properties of $Li_4Ti_5O_{12}$ as a lithium-ion battery anode material, *J. Power Sources*, 2013, **244**, 527.

43 J.-Y. Lin, C.-C. Hsu, H.-P. Ho and S.-H. Wu, Sol-gel synthesis of aluminum doped lithium titanate anode material for lithium ion batteries, *Electrochim. Acta*, 2013, **87**, 126.

44 H. Song, S.-W. Yun, H.-H. Chun, M.-G. Kim, K. Y. Chung, H. S. Kim, B.-W. Cho and Y.-T. Kim, Anomalous decrease in structural disorder due to charge redistribution in Cr-doped $Li_4Ti_5O_{12}$ negative-electrode materials for high-rate Li-ion batteries, *Energy Environ. Sci.*, 2012, **5**, 9903.

45 F. Wu, X. Li, Z. Wang and H. Guo, Synthesis of chromium-doped lithium titanate microspheres as high-performance anode material for lithium ion batteries, *Ceram. Int.*, 2014, **40**, 13195.

46 X. Li, M. Qu and Z. Yu, Structural and electrochemical performances of $Li_4Ti_{5-x}Zr_xO_{12}$ as anode material for lithium-ion batteries, *J. Alloys Compd.*, 2009, **487**, L12.

47 T.-F. Yi, B. Chen, H.-Y. Shen, R.-S. Zhu, A.-N. Zhou and H.-B. Qiao, Spinel $Li_4Ti_{5-x}Zr_xO_{12}$ ($0 \leq x \leq 0.25$) materials as high-performance anode materials for lithium-ion batteries, *J. Alloys Compd.*, 2013, **558**, 11.

48 Z. Wang, Z. Wang, W. Peng, H. Guo and X. Li, An improved solid-state reaction to synthesize Zr-doped $Li_4Ti_5O_{12}$ anode material and its application in $LiMn_2O_4/Li_4Ti_5O_{12}$ full-cell, *Ceram. Int.*, 2014, **40**, 10053.

49 T.-F. Yi, J. Shu, Y.-R. Zhu, X.-D. Zhu, C.-B. Yue, A.-N. Zhou and R.-S. Zhu, High-performance $Li_4Ti_{5-x}V_xO_{12}$ ($0 \leq x \leq 0.3$) as an anode material for secondary lithium-ion battery, *Electrochim. Acta*, 2009, **54**, 7464.

50 C.-C. Yang, H.-C. Hu, S. J. Lin and W.-C. Chien, Electrochemical performance of V-doped spinel $Li_4Ti_5O_{12}$/C composite anode in Li-half and $Li_4Ti_5O_{12}$/$LiFePO_4$-full cell, *J. Power Sources*, 2014, **258**, 424.

51 L. Shi, X. Hu and Y. Huang, Fast microwave-assisted synthesis of Nb-doped $Li_4Ti_5O_{12}$ for high-rate lithium-ion batteries, *J. Nanopart. Res.*, 2014, **16**, 2332.

52 M. Guo, S. Wang, L.-X. Ding, C. Huang and H. Wang, Tantalum-doped lithium titanate with enhanced

performance for lithium-ion batteries, *J. Power Sources*, 2015, **283**, 372.

53 Y. Qi, Y. Huang, D. Jia, S.-J. Bao and Z. P. Guo, Preparation and characterization of novel spinel $Li_4Ti_5O_{12-x}Br_x$ anode materials, *Electrochim. Acta*, 2009, **54**, 4772.

54 J. Wang, Z. Yang, W. Li, X. Zhong, L. Gu and Y. Yu, Nitridation Br-doped $Li_4Ti_5O_{12}$ anode for high rate lithium ion batteries, *J. Power Sources*, 2014, **266**, 323.

55 Z. Zhao, Y. Xu, M. Ji and H. Zhang, Synthesis and electrochemical performance of F-doped $Li_4Ti_5O_{12}$ for lithium-ion batteries, *Electrochim. Acta*, 2013, **109**, 645.

56 X. Han, Z. Zhao, Y. Xu, D. Liu, H. Zhang and C. Zhao, Synthesis and characterization of F-doped nanocrystalline $Li_4Ti_5O_{12}$/C compounds for lithium-ion batteries, *RSC Adv.*, 2014, **4**, 41968.

57 X. Guo, H. F. Xiang, T. P. Zhou, X. K. Ju and Y. C. Wu, Morphologies and structures of carbon coated on $Li_4Ti_5O_{12}$ and their effects on lithium storage performance, *Electrochim. Acta*, 2014, **130**, 470.

58 J. Wang, X.-M. Liu, H. Yang and X.-D. Shen, Characterization and electrochemical properties of carbon-coated $Li_4Ti_5O_{12}$ prepared by a citric acid sol-gel method, *J. Alloys Compd.*, 2011, **509**, 712.

59 Y. Ren, P. Lu, X. Huang, S. Zhou, Y. Chen, B. Liu, F. Chu and J. Ding, In-situ synthesis of nano-$Li_4Ti_5O_{12}$/C composite as an anode material for Li-ion batteries, *Solid State Ionics*, 2015, **274**, 83.

60 H.-G. Jung, J. Kim, B. Scrosati and Y.-K. Soon, Micron-sized, carbon-coated $Li_4Ti_5O_{12}$ as high power anode for advanced lithium batteries, *J. Power Sources*, 2011, **196**, 7763.

61 H. Liu, Y. Feng, K. Wang and J. Xie, Synthesis and electrochemical properties of $Li_4Ti_5O_{12}$/C composite by the PVB rheological phase method, *J. Phys. Chem. Solids*, 2008, **69**, 2037.

62 X. Li, P. Huang, Y. Zhou, H. Peng, W. Li, M. Qu and Z. Yu, A novel $Li_4Ti_5O_{12}$/graphene/carbon nano-tubes hybrid material for high rate lithium ion batteries, *Mater. Lett.*, 2014, **133**, 289.

63 Y. Yang, B. Qiao, X. Yang, L. Fang, C. Pan, W. Song, H. Hou and X. Ji, Lithium Titanate Tailored by Cathodically Induced Graphene for an Ultrafast Lithium Ion Battery, *Adv. Funct. Mater.*, 2014, **24**, 4349.

64 J. Zhang, Y. Cai, J. Wu and J. Yao, Graphene oxide-confined synthesis of $Li_4Ti_5O_{12}$ microspheres as high-performance anodes for lithium ion batteries, *Electrochim. Acta*, 2015, **165**, 422.

65 Y. Ding, G. R. Li, C. W. Xiao and X. P. Gao, Insight into effects of graphene in $Li_4Ti_5O_{12}$/carbon composite with high rate capability as anode materials for lithium ion batteries, *Electrochim. Acta*, 2013, **102**, 282.

66 X. Li, M. Qu and Z. Yu, Preparation and electrochemical performance of $Li_4Ti_5O_{12}$/graphitized carbon nanotubes composite, *Solid State Ionics*, 2010, **181**, 635.

67 Z. Wang, Z. Wang, W. Peng, H. Guo and X. Li, $Li_4Ti_5O_{12}$ co-modified with carbon nanotubes and pyrolytic carbon as an advanced anode material for lithium-ion batteries, *Mater. Lett.*, 2014, **137**, 413.

68 T. Liu, H. Ni, W.-L. Song and L.-Z. Fan, Enhanced electrochemical performance of $Li_4Ti_5O_{12}$ as anode material for lithium-ion batteries with different carbons as support, *J. Alloys Compd.*, 2015, **646**, 189.

69 S. Huang, Z. Wen, X. Zhu and Z. Gu, Preparation and electrochemical performance of Ag doped $Li_4Ti_5O_{12}$, *Electrochem. Commun.*, 2004, **6**, 1093.

70 S. Huang, Z. Wen, J. Zhang, Z. Gu and X. Xu, $Li_4Ti_5O_{12}$/Ag composite as electrode materials for lithium-ion battery, *Solid State Ionics*, 2006, **177**, 851.

71 S. Huang, Z. Wen, J. Zhang and X. Yang, Improving the electrochemical performance of $Li_4Ti_5O_{12}$/Ag composite by an electroless deposition method, *Electrochim. Acta*, 2007, **52**, 3704.

72 Y.-R. Zhu, T.-F. Yi, H.-T. Ma, Y.-Q. Ma, L.-J. Jiang and R.-S. Zhu, Improved electrochemical performance of Ag-modified $Li_4Ti_5O_{12}$ anode material in a broad voltage window, *J. Chem. Sci.*, 2014, **126**, 17.

73 Z. Liu, N. Zhang, Z. Wang and K. Sun, Highly dispersed Ag nanoparticles (<10 nm) deposited on nanocrystalline $Li_4Ti_5O_{12}$ demonstrating high-rate charge/discharge capability for lithium-ion battery, *J. Power Sources*, 2012, **205**, 479.

74 H. Ge, L. Chen, S. Lin, X. Shi and X.-M. Song, Advanced electrochemical performances of $Li_4Ti_5O_{12}$/Ag prepared by a facile synthesis route, *Ionics*, 2014, **20**, 1189.

75 J.-G. Kim, D. Shi, M.-S. Park, G. Jeong, Y.-U. Heo, M. Seo, Y.-J. Kim, J. H. Kim and S. X. Dou, Controlled Ag-driven superior rate-capability of $Li_4Ti_5O_{12}$ anodes for lithium rechargeable batteries, *Nano Res.*, 2013, **6**, 365.

76 G. B. Xu, W. Li, L. W. Yang, X. L. Wei, J. W. Ding, J. X. Zhong and P. K. Chu, Highly-crystalline ultrathin $Li_4Ti_5O_{12}$ nanosheets decorated with silver nanocrystals as a high-performance anode material for lithium ion batteries, *J. Power Sources*, 2015, **276**, 247.

77 A. Erdas, S. Ozcan, D. Nalci, M. O. Guler and H. Akbulut, Novel Ag/$Li_4Ti_5O_{12}$ binary composite anode electrodes for high capacity Li-ion batteries, *Surf. Coat. Technol.*, 2015, **271**, 136.

78 M. Krajewski, M. Michalska, B. Hamankiewicz, D. Ziolkowska, K. P. Korona, J. B. Jasinski, M. Kaminska, L. Lipinska and A. Czerwinski, $Li_4Ti_5O_{12}$ modified with Ag nanoparticles as an advanced anode material in lithium-ion batteries, *J. Power Sources*, 2014, **245**, 764.

79 M. Krajewski, B. Hamankiewicz and A. Czerwinski, Voltammetric and impedance characterization of $Li_4Ti_5O_{12}$/n-Ag composite for lithium-ion batteries, *Electrochim. Acta*, 2016, **219**, 277.

80 S. Huang, Z. Wen, B. Lin, J. Han and X. Xu, The high-rate performance of the newly designed $Li_4Ti_5O_{12}$/Cu composite anode for lithium ion batteries, *J. Alloys Compd.*, 2008, **477**, 400.

81 C. Cheng, H. Liu, X. Xue, H. Cao and L. Shi, Highly dispersed copper nanoparticle modified nano $Li_4Ti_5O_{12}$ with high rate performance for lithium ion battery, *Electrochim. Acta*, 2014, **120**, 226.

82 N. Li, J. Liang, D. Wei, Y. Zhu and Y. Qian, Solvothermal synthesis of micro-/nanoscale Cu/$Li_4Ti_5O_{12}$ composites for high rate Li-ion batteries, *Electrochim. Acta*, 2014, **123**, 346.

83 Q. Wang, W. Liu, J. Zhang, X. Xie and B. Xia, Performance of electroless-plated lithium titanate/copper composites as anode materials in 18650-type lithium-ion batteries, *J. Solid State Electrochem.*, 2015, **19**, 1411.

84 A. Erdas, S. Ozcan, M. O. Guler and H. Akbulut, Sol-Gel Synthesis of Nanocomposite Cu-$Li_4Ti_5O_{12}$ Structures for Ultrahigh Rate Li-Ion Batteries, *Acta Phys. Pol., A*, 2015, **127**, 1026.

85 W. Wang, Y. Guo, L. Liu, S. Wang, X. Yang and H. Guo, Gold coating for a high performance $Li_4Ti_5O_{12}$ nanorod aggregates anode for lithium-ion batteries, *J. Power Sources*, 2014, **245**, 624.

86 K.-S. Park, A. Benayad, D.-J. Kang and S.-G. Doo, Nitridation-Driven Conductive $Li_4Ti_5O_{12}$ for Lithium Ion Batteries, *J. Am. Chem. Soc.*, 2008, **130**, 14930.

87 X. Zhao, Q. Zhou, H. Ming, J. Adkins, M. Liu, L. Su and J. Zheng, Surface nitridation induced high electrochemical performance of $Li_4Ti_5O_{12}$ using urea as a nitrogen source, *Ionics*, 2013, **19**, 1843.

88 H. Park, T. Song, H. Han and U. Paik, Electrospun $Li_4Ti_5O_{12}$ nanofibers sheathed with conductive TiN/TiO_xN_y layer as an anode for high power Li-ion batteries, *J. Power Sources*, 2013, **244**, 726.

89 J. Shu, M. Shui, F. Huang, D. Xu, Y. Ren, L. Hou, J. Cui and J. Xu, Comparative study on surface behaviors of copper current collector in electrolyte for lithium-ion batteries, *Electrochim. Acta*, 2011, **56**, 3006.

90 S.-T. Myung, Y. Hitoshi and Y.-K. Sun, Electrochemical behavior and passivation of current collectors in lithium-ion batteries, *J. Mater. Chem.*, 2011, **21**, 9891.

91 Y. Zhu and C. Wang, Novel CV for Phase Transformation Electrodes, *J. Phys. Chem. C*, 2011, **115**, 823.

92 D. Linden and T. B. Reddy, *Handbook of Batteries*, McGraw-Hill, New York, 2002.

93 A. J. Bard and L. R. Faulkner, *Electrochemical methods: fundamentals and applications*, John Willey & Sons, Inc., New York, 2001.

94 N. Takami, K. Hoshina and H. Inagaki, Lithium Diffusion in $Li_{4/3}Ti_{5/3}O_4$ Particles during Insertion and Extraction, *J. Electrochem. Soc.*, 2011, **158**, A725.